

The nature of convectively unstable waveguide mode disturbances on the magnetospheric flanks

Andrew N. Wright

Mathematical Institute, University of St. Andrews, St. Andrews, Fife, UK

Katharine J. Mills

Thompson Marconi Sonar Ltd., Stockport, Cheshire, UK

Aaron W. Longbottom

Fluid Gravity Engineering Ltd., St. Andrews, Fife, UK

Michael S. Ruderman

Department of Applied Mathematics, University of Sheffield, Sheffield, UK

Received 1 October 2001; revised 20 March 2002; accepted 1 May 2002; published 19 September 2002.

[1] Convectively unstable disturbances are often described in terms of propagating wave packets that grow and broaden. We extend such a description here and show how it recovers previous results and agrees with simulations. Applying these ideas to the magnetospheric flanks, we find that such wave packets will often not provide a driver of long enough duration for establishing a fully formed field line resonance (FLR). This suggests that the alternative description of the convective instability as a steady wave train radiated by a fixed source may be more appropriate for the flanks on some occasions. Whether the unstable waveguide modes prefer to exist as steady wave trains or convecting wave packets can have important implications for identifying the mechanisms through which the magnetosheath is coupled to the magnetosphere. *INDEX TERMS:* 2752 Magnetospheric Physics: MHD waves and instabilities; 2784 Magnetospheric Physics: Solar wind/magnetosphere interactions; 7827 Space Plasma Physics: Kinetic and MHD theory; 7871 Space Plasma Physics: Waves and instabilities

Citation: Wright, A. N., K. J. Mills, A. W. Longbottom, and M. S. Ruderman, The nature of convectively unstable waveguide mode disturbances on the magnetospheric flanks, *J. Geophys. Res.*, 107(A9), 1242, doi:10.1029/2001JA005091, 2002.

1. Introduction

1.1. History

[2] Ultralow frequency (ULF) waves are a natural and readily observable feature of the terrestrial magnetosphere. Understanding subtle, yet persistent, properties of these waves has a long history of providing considerable insight into the structure of the magnetosphere and its dynamic interaction with the solar wind. For example, the *Samson et al.* [1971] recognition of polarization changes with latitude and across noon led to the field line resonance (FLR) model of *Southwood* [1974] and *Chen and Hasegawa* [1974], in which a monochromatic fast magnetopause surface mode couples resonantly to an Alfvén wave on a specific L-shell. Observations also showed that certain discrete frequencies are preferred, and this led *Kivelson and Southwood* [1985] to suggest the fast modes were not Kelvin–Helmholtz driven magnetopause surface waves, as originally suggested, but global cavity modes of the magnetosphere. The latter would naturally provide a set of discrete driving frequencies.

[3] Recently the open nature of the magnetosphere cavity has been included by describing the flanks as a waveguide [*Samson et al.*, 1992; *Walker et al.*, 1992; *Wright*, 1994]. The observed increase in ULF wave activity when the solar wind speed at the Earth's orbit exceeds 500 km s^{-1} [*Engbreton et al.*, 1998] is supportive of the studies which suggest the waveguide modes may be excited by the kinetic energy of the magnetosheath plasma via a Kelvin–Helmholtz process [*McKenzie*, 1970; *Fujita et al.*, 1996; *Walker*, 1998; *Mann et al.*, 1999; *Mills et al.*, 1999]. Indeed, this excitation process may generate several FLRs simultaneously, and *Mills and Wright* [1999] note they should all have the same azimuthal phase speed. *Mann and Wright* [1999] showed this property was present in previous work which had reported simultaneous FLRs [*Ziesolleck and McDiarmid*, 1994; *Fenrich et al.*, 1995] and showed how, even when the phase speeds were different, the likely driving mechanism of the waveguide modes could be deduced. *Mathie and Mann* [2000] used these ideas to analyze ground based magnetometer data and found a preference for the Kelvin–Helmholtz mechanism to operate on the dawn flank.

[4] Numerical methods have proved to be of great importance for increasing our understanding of the role of the

Kelvin–Helmholtz instability. Most studies have focused on the Kelvin–Helmholtz surface wave, as this is the most unstable mode, and began with normal mode calculations [Southwood, 1968; Walker, 1981; Miura and Pritchett, 1982]. The nonlinear evolution of the surface mode has been investigated in several simulations using a periodic domain [Miura, 1984, 1987, 1992, 1995] and also non-periodic domains [Wu, 1986; Manuel and Samson, 1993]. The most recent studies have addressed the Kelvin–Helmholtz excitation of linear waveguide modes in a nonperiodic waveguide [Mills *et al.*, 2000], and their subsequent nonlinear behavior in a periodic waveguide [Keller and Lysak, 2001]. These studies confirm that it is important to consider whether small disturbances are convectively unstable or absolutely unstable, as suggested by Wright *et al.* [2000].

1.2. Absolute and Convective Instabilities

[5] The theory of absolute and convective instabilities has been developed in other areas of plasma physics by Briggs [1964], and the interested reader is referred to the review by Bers [1983] for a comprehensive list of references. Here we only summarize the qualitative behavior [see also Wright *et al.*, 2000]. A localized initial disturbance may be regarded as a wave packet, whose subsequent evolution consists of propagation (with the group velocity, V_g) and also wave packet broadening and amplitude growth for an unstable solution. The frame from which we view this growing and broadening wave packet is crucial in determining the ultimate behavior of the system. Suppose we transform to a frame that moves with the wave packet: In this frame the wave packet does not appear to move, but it does grow in amplitude and broaden. If we choose any fixed point in this frame and wait long enough the wave packet will eventually engulf this point and the amplitude of the disturbance at that fixed point will become infinite as $t \rightarrow \infty$. This is the definition of an absolute instability.

[6] The situation may be quite different when considered from a different frame, say one in which the wave packet has a large group velocity compared to the rate of broadening. The wave packet grows and broadens just as before, but now propagates away so rapidly that it will leave its initial location undisturbed. Indeed, if we choose any fixed point in this new frame and wait long enough ($t \rightarrow \infty$) that point will be left undisturbed. In this frame the wave packet is said to be convectively unstable. There is, of course, a continuum of frames of reference (characterized by a speed V_f relative to some absolute frame) from which we could view the wave packet. It turns out that the first frame we considered (moving with the wave packet, $V_f = V_g$) has the largest growth rate as $t \rightarrow \infty$, and this is equal to the maximum growth rate of that particular normal mode. If V_f differs slightly from V_g the wave packet moves away slowly, and at a fixed point in this new frame we would observe a slightly reduced growth rate as $t \rightarrow \infty$. Thus the observed asymptotic growth rate is a function of frame, $\gamma(V_f)$, and when V_f differs sufficiently from V_g the growth rate first falls to zero and then becomes negative. When $\gamma(V_f)$ is negative we are in a frame for which the wave packet is convectively unstable.

[7] An alternative interpretation of the difference between absolutely and convectively unstable frames of reference is in terms of a localized steady harmonic driving source

varying as $\exp(-i\omega t)$. We can think of this source as launching a series of wave packets. In an absolutely unstable frame, the wave packets grow and broaden to fill all space as $t \rightarrow \infty$ just as before. In a convectively unstable frame each wave packet will grow as it convects away from the source. Superposing successive wave packets leads to the generation of a wave train leaving the source region and growing exponentially with distance from the source. This is sometimes referred to as the signaling problem, and the wave train has the structure of a normal mode with frequency equal to the driving frequency and complex wave number determined by the dispersion relation.

1.3. Application to the Magnetosphere

[8] The Kelvin–Helmholtz surface mode is convectively unstable on the dayside and flanks. A simulation by Manuel and Samson [1993] demonstrated the signaling problem behavior: they continually disturbed the subsolar point and observed the growing wave train that propagated around the flanks to have an e-folding length of the order of an Earth radius (R_E). Wright *et al.* [2000] applied the absolute and convective instability analysis of Briggs [1964] and found a similar spatial growth. The surface mode will grow to nonlinear amplitudes as it propagates antisunward, and this may well account for the broadening of the velocity shear layer on the flanks [Manuel and Samson, 1993].

[9] Wright *et al.* [2000] and Mills *et al.* [2000] found that waveguide mode wave packets would be convectively unstable on the flanks and have an e-folding length of about $20 R_E$. Consequently, waveguide mode disturbances will not grow to nonlinear amplitudes as they propagate antisunward, and this may explain why such waves are so elusive in data. Indeed the main observational evidence for these waves is the FLRs they are thought to excite, although Mann *et al.* [1998] have reported a rare example.

[10] It is likely that whether or not the waveguide modes are unstable in practice will be influenced by the magnetosheath magnetic field. In the study by Fujita *et al.* [1996] a significant stabilizing effect was produced by this field: They found that sheath flow speeds in excess of 800 km s^{-1} are required for instability, which will seldom occur. In contrast, the absence of a stabilizing sheath field orientation in normal mode calculations [Mann *et al.*, 1999; Mills *et al.*, 1999] and both linear [Mills *et al.*, 2000] and nonlinear [Keller and Lysak, 2001] simulations indicate a lower sheath flow threshold of $\sim 500 \text{ km s}^{-1}$ which can be exceeded during strong solar wind flow.

[11] In this paper we consider the nature of the convectively unstable waveguide mode disturbances. We derive accurate asymptotic expressions for the shape of the wave packet and show how this can be used to recover an approximate $\gamma(V_f)$ relation that determines the absolute or convective behavior of the instability. We then consider the properties of FLRs that would be excited by both waveguide mode wave packets and spatially growing steady wave trains in an effort to understand the manner in which solar wind excites the magnetosphere.

2. Model

[12] The model we adopt is a Cartesian waveguide representation of the flank which is described in detail by

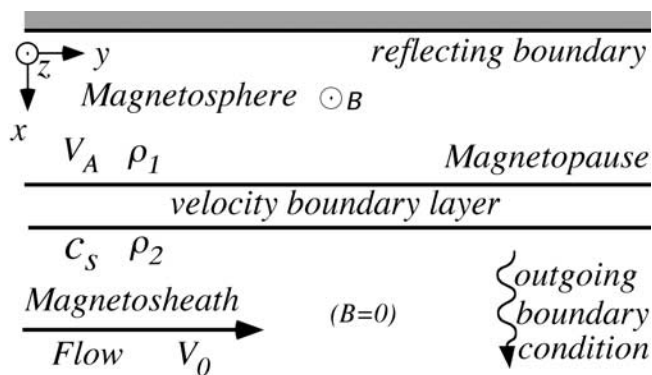


Figure 1. The model of the magnetospheric waveguide on the flank viewed in the magnetospheric rest frame.

Mills et al. [2000] and *Wright et al.* [2000]. Here we give a brief summary: Figure 1 depicts the dusk flank waveguide with y representing the azimuthal coordinate increasing from noon to late evening. The magnetosphere is taken to be a uniform stationary cold plasma with an inner reflecting boundary to represent the turning point that waveguide modes have in a nonuniform magnetosphere. The magnetosheath is represented by a uniform hot plasma moving with speed v_0 antisunward. The radial and field aligned coordinates may be identified with x and z , respectively. The magnetospheric plasma rest frame is taken as our absolute frame of reference against which all other velocities are measured. The equilibrium flow changes smoothly over a shear layer of width 2δ , which is centered on $x = d$. The depth of the magnetospheric waveguide (d) is taken to be $10 R_E$ ($R_E =$ an Earth radius) on the flanks, and all lengths are normalized by this quantity. Velocities are normalized by the magnetosheath sound speed ($\sim 100 \text{ km s}^{-1}$), giving a time normalization of 640 seconds or 10.5 minutes.

[13] Several points should be noted regarding our simplified model. As mentioned above, our model represents the flanks of the magnetosphere, and in particular the low latitude section which will be the most unstable (since the magnetospheric magnetic field is perpendicular to magnetosheath velocity here). Although we assume an infinitely long waveguide in our model, this is purely for mathematical convenience, and our results should not be used to interpret the behavior of waves antisunward of the flank in the magnetotail where a different model is required [*Mills et al.*, 1999]. Also the transition from flank to tail would require a three-dimensional equilibrium configuration. This is beyond the scope of the present calculation which can strictly be only applied to evolution of waves locally on the flanks.

[14] The Kelvin–Helmholtz surface mode, which has received considerable attention in the past, has an e-folding length on the flanks of the order of an R_E . Thus the surface mode will grow to nonlinear amplitudes as it propagates around the flanks. The surface mode vortices have a tendency to merge as they move tailward and form larger scale boundary features, as noted by *Miura* [1999] and *Manuel and Samson* [1993]. The effect of the surface mode is to broaden the Low-Latitude Boundary Layer (LLBL), and transfer energy and momentum from the magnetosheath to the magnetospheric plasma close to the magnetopause.

[15] The Kelvin–Helmholtz surface mode will not transfer energy deep into the magnetosphere, however Kelvin–Helmholtz excited waveguide modes can as they are able to propagate through the body of the magnetosphere. In this paper we focus on the properties of the recently discovered Kelvin–Helmholtz waveguide modes, and so represent the effect of the more unstable surface mode phenomenologically as the broadened boundary layer that it produces in its nonlinear phase on the flanks. As mentioned above, the convectively unstable waveguide modes should remain linear on the flanks which is the region of interest in this paper.

[16] Our work builds upon the investigations of *Mann et al.* [1999], *Mills et al.* [1999, 2000], and *Wright et al.* [2000], in which the fact that the magnetosheath flow could excite (Kelvin–Helmholtz) unstable waveguide modes was established. For waveguide modes to exist it is necessary to have an efficient reflecting boundary condition in the inner magnetosphere. In the present model (which was also employed in the studies listed above) we simply impose a reflection point at a distance of $10 R_E$ in from the magnetopause. In reality, reflection occurs at a turning point associated with the increase in Alfvén speed as the Earth is approached. Indeed, *Mills and Wright* [1999] used a nonuniform magnetosphere in which the waves had a turning point, rather than the uniform magnetosphere employed here with a reflection point. This has the effect of shifting the waveguide frequencies slightly since the phase change at the reflection point, Alfvén speed, and effective depth of the waveguide all differ in the two models. However, both models show the same physical excitation processes operate in the uniform and nonuniform waveguides, and so we employ the simpler uniform model here to help identify the essential physics involved. The reader is referred to the works of *Mills et al.* [1999] and *Wright et al.* [2000] for further discussion of the model used here and its applicability.

3. Simulations

[17] To illustrate the behavior of convectively unstable disturbances we consider some results from the numerical scheme described by *Mills et al.* [2000]. When the (normalized) change of equilibrium flow across the shear layer is not too high ($\Delta V = 2.0$) the surface mode is unstable, but all the waveguide modes are stable. This situation is likely to occur close to noon for strong solar wind flow or on the flanks during more moderate conditions [see *Mann and Wright*, 1999, Figure 1].

[18] The dispersion relation for the surface mode has been solved numerically [see *Mills et al.*, 2000, Figure 4], and we reproduce the $\Delta V = 2.0$, $\delta = 0.1$ result here in Figure 2. The component of the wave number in the y direction is real and denoted by k , (the z component is taken to the zero). Figure 2b shows the fastest growing surface mode has $k = k_m = 4.625$, and we seed the simulations with a localized wave packet in y containing a couple of cycles at this wave number. Figure 2a contains the variation of ω_r with k , from which we determine the group velocity of the wave packet by $V_{gm} = V_g(k_m) = \partial\omega_r(k_m)/\partial k = 0.9861$. If the wave packet is centered on $y = 0$ when $t = 0$, it should be centered on $y = V_{gm}t$ at later times. For computation

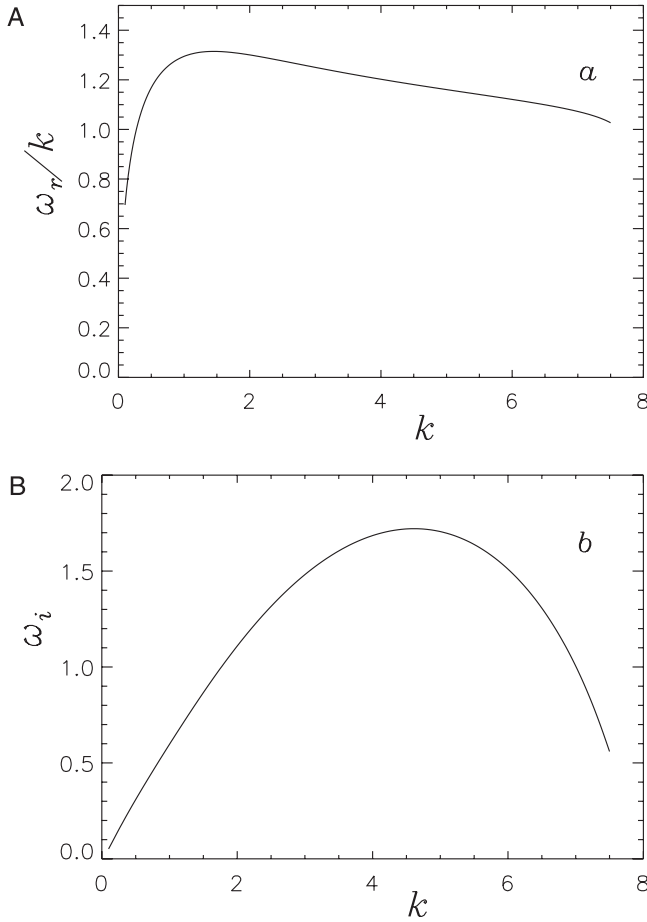


Figure 2. The dispersion relation for the fast surface mode when $\Delta V = 2.0$ and $\delta = 0.1$. The wave number in the y direction is k .

convenience, we transform to a frame y' for the simulation where

$$y' = y - V_f t \quad (1)$$

so the wave packet should be centered on

$$y' = (V_{gm} - V_f)t. \quad (2)$$

V_f is the velocity of the y' origin relative to the (absolute) magnetospheric rest frame. Evidently, choosing $V_f = V_{gm}$ we transform to a frame moving with the wave packet group velocity, so the wave packet then appears to be at rest and remains centered in our computational domain. We chose $V_f = 1.0$, so the wave packet should drift very slowly (at a velocity of -0.014) in our simulation frame.

[19] Figure 3 shows the snapshot of the x component of the velocity in y' frame along $x = 0.75$ at $t = 60.0$, at which time we expect the wave packet to be centered on $y' = -0.84$. The wave number of the oscillations measured from this plot actually varies by about 10 percent from over $-10 < y' < 10$, but has a value of 4.7 at the center, in good agreement with $k_m = 4.625$. A notable feature of Figure 3 is the Gaussian profile of the envelope. We observed that this form was independent of the initial

profile, suggesting that an asymptotic treatment may be useful for describing the properties of a whole range of initial conditions.

4. Asymptotic Behavior

4.1. Wave Packet Properties

[20] We can express the variation of perturbations in (y, t) as a Fourier integral over real k ,

$$f(y, t) = \int_{-\infty}^{+\infty} A(k) e^{\omega_i(k)t + i(ky - \omega_r(k)t)} dk \quad (3)$$

f could represent the x component of velocity (as in Figure 3) or the compressional magnetic field component. (Note that there is also an x -dependence which is simply that of the normal mode. However, we omit this term here as we are considering only the variation in the y direction.) The complex eigenfrequency of the normal mode $\omega(k) = \omega_r(k) + i\omega_i(k)$ varies with k as shown in Figure 2. We anticipate that the fastest growing modes in (3) will dominate, so expand the integrand about k_m , where $\partial\omega_i(k_m)/\partial k = 0$. The Taylor series for $\omega(k)$ give

$$\omega_r(k) = \omega_{rm} + V_g \tilde{k} + \beta \tilde{k}^2 + \dots \quad (4a)$$

$$\omega_i(k) = \omega_{im} - \alpha \tilde{k}^2 + \dots \quad (4b)$$

where $\tilde{k} = k - k_m$, $\omega_m = \omega(k_m)$, $\alpha = -\frac{1}{2}\partial^2\omega_i(k_m)/\partial k^2$, $\beta = \frac{1}{2}\partial^2\omega_r(k_m)/\partial k^2$, and $V_g = \partial\omega_r(k_m)/\partial k$ is the group velocity of the wave packet. Substituting (4a) and (4b) into (3) and collecting terms yields

$$f(y, t) = A(k_m) \exp[\omega_{im}t + i(k_m y - \omega_{rm}t)] \cdot \int_{-\infty}^{+\infty} \exp[i(y - V_g t)\tilde{k} - \Delta^2 \tilde{k}^2 t] d\tilde{k} \quad (5)$$

where

$$\Delta^2 = \alpha + i\beta, \quad \text{Re}\{\Delta\} > 0 \quad (6)$$

Note that the maximum exponential growth at $k = k_m$ means that as time increases the solution is dominated by an

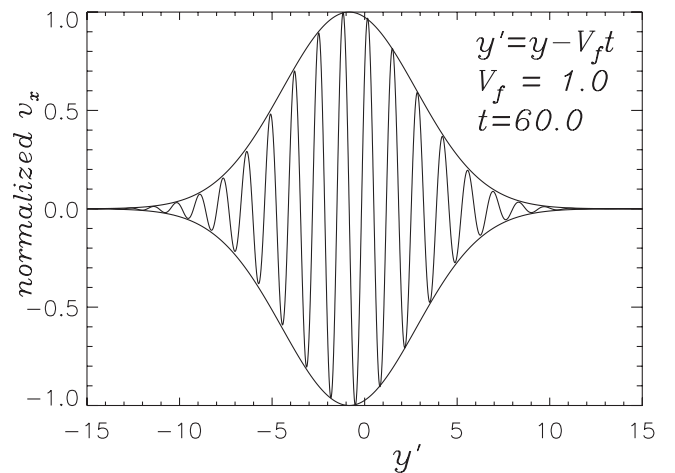


Figure 3. A snapshot of the (normalized) v_x in the y' frame ($V_f = 1.0$) for the surface mode ($\Delta V = 2.0$, $\delta = 0.1$, $x = 0.75$, $t = 60.0$). The Gaussian envelope is predicted by the wave packet analysis.

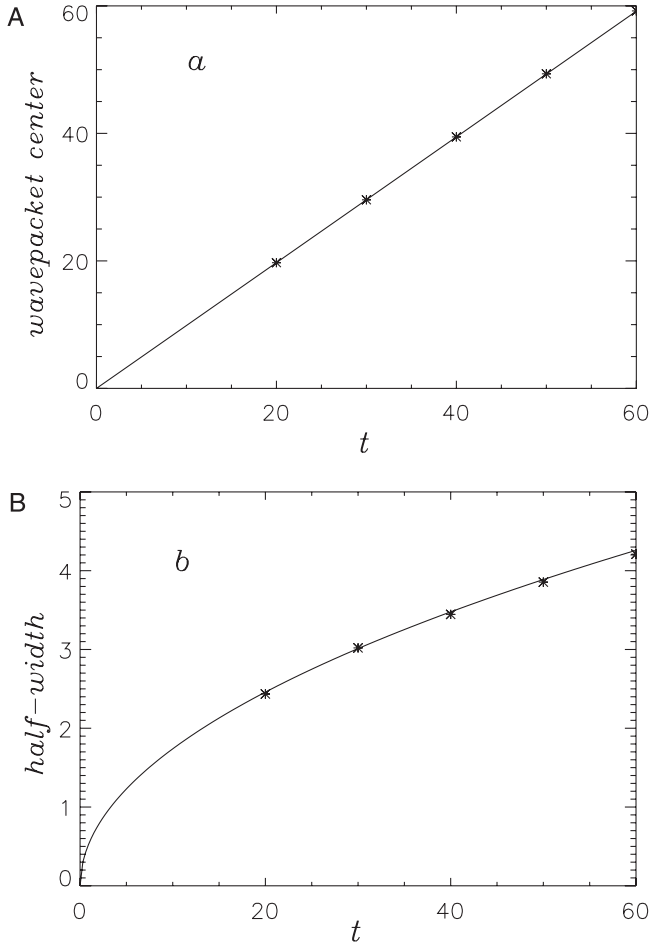


Figure 4. A comparison of (a) the location of the wave packet center (in the y frame) and (b) its full width at half maximum as a function of time for the simulation (stars) and the analytic result (line).

increasingly narrow ($\propto 1/\sqrt{t}$) band of wave numbers centered on k_m . For this reason we are able to neglect the second term in the Taylor series of $A(k)$, which does not affect the leading solution we derive below. The integral in (5), after completing the square of the exponent, becomes

$$\exp\left[-\frac{(y-V_g t)^2}{4\Delta^2 t}\right] \times \int_{-\infty}^{+\infty} \exp\left[\left(i\Delta t^{1/2}\tilde{k} + \frac{(y-V_g t)}{2\Delta t^{1/2}}\right)^2\right] d\tilde{k} \quad (7)$$

The integral in (7) is equal to $\sqrt{\pi/t}/\Delta$, and combining the above relations gives.

$$f(y, t) \propto \frac{1}{\sqrt{t}} \exp\left[\omega_{im} t + i(k_m y - \omega_{rm} t) - \frac{(y-V_g t)^2}{4\Delta^2 t}\right] \quad (8)$$

[21] The terms in the exponent denote, respectively, temporal growth of the envelope, phase motion within the envelope and a Gaussian profile that translates with a speed equal to the group velocity and has a width increasing as

\sqrt{t} . The Gaussian term requires a little care as the length scale (which is proportional to Δ) is complex.

[22] Writing

$$\frac{1}{\Delta^2} = a + ib \equiv \frac{\alpha}{\alpha^2 + \beta^2} - \frac{i\beta}{\alpha^2 + \beta^2} \quad (9)$$

we find

$$f(y, t) \propto \frac{1}{\sqrt{t}} \exp\left[\omega_{im} t - \frac{a}{4t} (y - V_g t)^2\right] \times e^{i\phi} \quad (10)$$

where

$$\phi = \left(k_m + \frac{bV_g}{2} - \frac{by}{4t}\right)y - \left(\omega_{rm} + \frac{b}{4}V_g^2\right)t \quad (11)$$

[23] Note that when the length scale ($\Delta t^{1/2}$) has an imaginary part ($b \neq 0$), the frequency and wave number are shifted slightly from ω_{rm} and k_m .

[24] According to (10) the wave packet has a Gaussian shape which is centered on $y = V_g t$ and has a half width at half maximum of $y_h = \sqrt{t \ln 16/a}$. From the surface mode dispersion relation (Figure 2) we calculate $k_m = 4.625$, $\omega_{im} = 1.7208$, $\omega_{rm} = 5.4381$, $V_g = 0.9861$, $\partial^2 \omega_r(k_m)/\partial k^2 = -0.06352$, $\partial^2 \omega_i(k_m)/\partial k^2 = -0.19765$, giving $a = 9.1719$ and $b = 2.9474$. Using these parameters we predict the location (in y) of the wave packet center and its width as functions of t . These are plotted in Figure 4, as lines. The stars correspond to measurements made from simulation results like that shown in Figure 3, after transforming from y' (the simulation frame) to y (the magnetospheric frame) using (1) with $V_f = 1.0$. The Gaussian envelope plotted in Figure 3 was calculated using (10) and is an excellent fit to the simulations. (The estimated half width and that measured from the simulation agreed to 1% or better, and the wave packet center is estimated to move at a speed of 0.9868 from the simulation which agrees well with the expected group velocity of 0.9861.)

4.2. Growth Rates

[25] The temporal growth rate of the disturbance at fixed y is found from the argument of the first exponential in (10). For large t the leading order behavior is $(\omega_{im} - aV_g^2/4)t$, indicating the growth rate in the y frame is $\gamma(V_f = 0) = \omega_{im} - aV_g^2/4 = -0.509$. It is significant that $\gamma(0) < 0$, as this means waiting long enough ($t \rightarrow \infty$) at fixed y (in the magnetosphere rest frame) the disturbance will tend to zero. As mentioned in section 1.2, this is the signature of a convective instability, where the wave packet moves off to infinity sufficiently swiftly. The situation is quite different in other frames, and the disturbance in the y' frame may be found by transforming (8) according to (1)

$$f(y', t) \propto \frac{1}{\sqrt{t}} \exp\left[\omega_{im} t + i(k_m y' - \omega'_{rm} t) - \frac{(y' - (V_g - V_f)t)^2}{4\Delta^2 t}\right] \quad (12)$$

where $\omega'_{rm} = \omega_{rm} - k_m V_f$ is the Doppler shifted real frequency at k_m . Expanding the quadratic in (12), employing

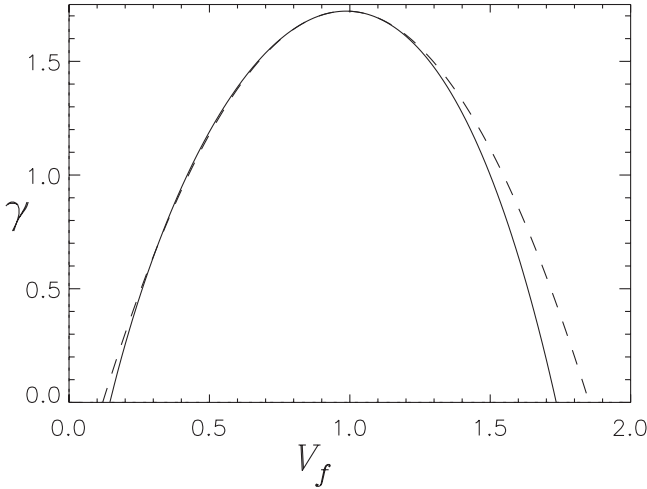


Figure 5. The asymptotic growth rate of surface mode disturbances as a function of reference frame speed. The solid line is the exact double root solution and the dashed line is the wave packet approximation ($\Delta V = 2.0$, $\delta = 0.1$).

(9), and collecting real and imaginary terms yields the result

$$f(y', t) \propto \frac{1}{\sqrt{t}} \exp \Phi \exp i \Psi \quad (13)$$

where

$$\Phi = \left[\omega_{im} - \frac{a}{4} (V_g - V_f)^2 \right] t + \frac{a}{4} [2(V_g - V_f) - y' t] y' \quad (14a)$$

$$\Psi = \left[k_m + \frac{b}{2} (V_g - V_f) - \frac{b y'}{4 t} \right] y' - \left[\omega'_{rm} + \frac{b}{4} (V_g - V_f)^2 \right] t \quad (14b)$$

Note how setting $V_f = 0$ in (13) and (14a) and (14b) recovers the results in (10) and (11).

[26] The theory of absolute and convective instabilities relies upon determining the asymptotic growth rate of wave packets at fixed y' as $t \rightarrow \infty$. In this limit $\Phi/t \rightarrow \gamma(V_f)$, and we may use (14a) to determine $\gamma(V_f)$

$$\gamma(V_f) = \omega_{im} - \frac{a}{4} (V_g - V_f)^2 \quad (15)$$

If $\gamma(V_f) > 0$ the frame has an absolute instability, and if $\gamma(V_f) < 0$ the instability is convective. The transition between the two occurs when $\gamma = 0$, i.e.,

$$\pm 2 \sqrt{\frac{\omega_{im}}{a}} = V_g - V_f \quad (16)$$

So we predict absolute instabilities when

$$V_g - 2 \sqrt{\frac{\omega_{im}}{a}} < V_f < V_g + 2 \sqrt{\frac{\omega_{im}}{a}} \quad (17)$$

Evidently a frame moving with the group velocity ($V_f = V_g$) will be absolutely unstable, and (15) indicates that the

asymptotic growth rate will be equal to the maximum growth rate of a normal mode with real k which is a familiar result from the formal instability analysis [Briggs, 1964; Bers, 1983]. Their method, which is based upon the behavior of double roots of the dispersion relation ($D(\omega, k) = \partial D(\omega, k) / \partial k = 0$), has been summarized by Mills *et al.* [2000] and used to calculate the surface mode growth rate. The solid curve in Figure 5 is reproduced from the work of Mills *et al.* [2000, Figure 5], and the dashed curve is the estimate of the growth rate based upon (15). The two estimates show very good agreement, and this is due to the surface mode dispersion relations (Figure 2), being approximated well by the quadratic Taylor series (4a) and (4b). Indeed, it is easy to prove that if the dispersion relations are represented exactly by (4a) and (4b), then the double root method would give (15): we write the dispersion relation as $D(\omega, k) = 0$, where we now assume

$$D(\omega, k) = \omega - \omega_{rm} - i\omega_{im} - V_g(k - k_m) + i\Delta^2(k - k_m)^2 \quad (18)$$

In the y' frame, where $\omega' = \omega - kV_f$, the dispersion relation becomes

$$D(\omega' + kV_f, k) = \omega' - \omega'_{rm} - i\omega_{im} + (V_f - V_g)(k - k_m) + i\Delta^2(k - k_m)^2 \quad (19)$$

and again $\omega'_{rm} = \omega_{rm} - k_m V_f$. Taking the derivative gives

$$\frac{\partial D}{\partial k} = (V_f - V_g) + 2i\Delta^2(k - k_m) \quad (20)$$

The double roots satisfy $D = \partial D / \partial k = 0$, so (19) and (20) provide two simultaneous equations for ω' and k whose solutions are

$$k = k_m + \frac{i}{2\Delta^2} (V_f - V_g) \quad (21a)$$

$$\omega' = \omega'_{rm} + i\omega_{im} - \frac{i}{4\Delta^2} (V_g - V_f)^2 \quad (21b)$$

The double root analysis shows the solution as $t \rightarrow \infty$ is $t^{-1/2} \exp i(ky' - \omega't)$ with ω' and k given in (21a) and (21b). The growth rate in the y' frame is simply the imaginary part of (21b), and recalling (19) it can be seen that this reproduces the result in (15) based upon our wave packet analysis. Indeed, the asymptotic result from the ω' and k in (21a) and (21b) substituted in $t^{-1/2} \exp i(ky' - \omega't)$ produces exactly the wave packet solution in (13) and (14a) and (14b) when terms proportional to $1/t$ are neglected. This corresponds to taking the limit $t \rightarrow \infty$, which is implicit in the double root analysis, and suggest our wave packet analysis may be useful in studying the solution at finite times and for considering how the solution tends to the asymptotic result.

[27] The above comparison shows that when the dispersion relation has a quadratic variation (4a) and (4b) the wave packet analysis (in the limit $t \rightarrow \infty$) reproduces exactly the double root analysis. This indicates that the discrepancy between the two estimates for $\gamma(V_f)$ shown in Figure 5 are due to the dispersion relation not being quadratic. In this sense, the neglect of higher order terms in the Taylor series (4a) and (4b) represents an error which

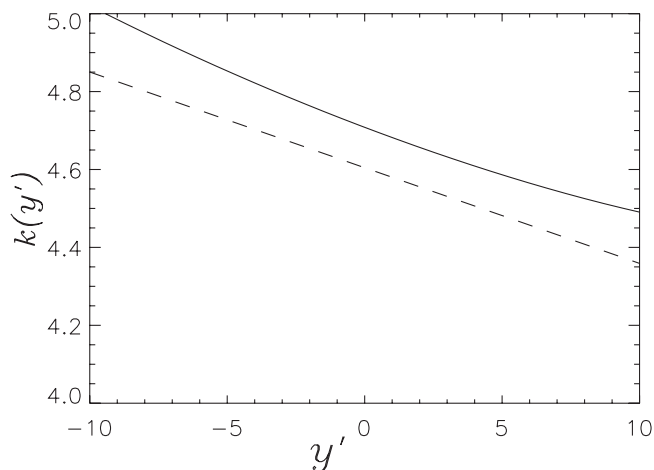


Figure 6. The variation of the local wave number of the oscillations in Figure 3 (solid line) and the analytic result of (22) (dashed line).

results in the difference evident in Figure 5. If higher order terms are included in the Taylor series we anticipate that even better agreement would be found in Figure 5.

4.3. Length Scales

[28] Besides the width of the wave packet, which we have already discussed, the other obvious length scale in Figure 3 is the wavelength of the phase oscillations within the envelope. The wavelength looks uniform across the wave packet, by eye, but a careful determination of the locations of the zeros of the oscillation enables us to calculate the local wavelength, and thus wave number which is plotted as the solid line in Figure 6. From the wave packet expressions in (13) and (14a) and (14b) we can also estimate k ,

$$k(y', t) \approx \frac{\partial \Psi}{\partial y} = k_m + \frac{b}{2}(V_g - V_f) - \frac{by'}{2t} \quad (22)$$

which shows the, perhaps, surprising result, that the local wave number varies linearly with y' . In the limit $t \rightarrow \infty$, k becomes constant. The dashed line in Figure 6 is a plot of (22) at $t = 60$, which differs from the simulation result by $\delta k \approx 0.13$. This discrepancy corresponds to a difference in the simulation and predicted wavelengths of 0.035, and since the grid resolution of the simulation was 0.025, it would appear that we can not determine the wavelength any more accurately. Thus the discrepancy in Figure 6 is probably due to numerical resolution.

5. Waveguide Wave Packets

[29] From the comparison of the wave packet solution with simulations (Figures 3 and 4) and with asymptotic results (Figure 5) we can have confidence that the theory provides a useful and reliable guide to the location, amplitude, phase structure and width of the wave packet, as well as the structure of the oscillations it contains. We shall now employ these results to study the properties of wave packets associated with waveguide modes that are believed to couple to FLRs.

[30] The Fourier integral in (3) describes the evolution of one $\omega(k)$ mode. When a system can support several modes,

such as in waveguide, $\omega(k)$ is multivalued and considering each $\omega_n(k)$ individually corresponds to looking at the behavior of each mode separately. It is important to realize that the full solution corresponds to the superposition of the Fourier integral of each mode. (The equilibrium used to construct the solutions in section 4 had only one unstable mode since $\Delta V = 2.0$.) Thus the absolute or convective nature of the system depends entirely upon the behavior of the surface mode that was considered.

[31] In an equilibrium with larger ΔV we find several modes can be unstable, and the range of V_f for which a given mode has a positive $\gamma(V_f)$, according to (15), will be different from the others in general. (This behavior is shown clearly in the work of *Mills et al.* [2000, Figure 13].) Thus any definitive statement on the absolute or convective instability of a system in a particular frame must be made by considering behavior of all unstable modes.

[32] The results of section 4 give us confidence that the wave packet description is accurate and reliable, so we now use this approximation to study the behavior of waveguide mode wave packets. Figure 7 shows the dispersion relations for the fundamental (solid line) and second harmonic (dashed line) waveguide mode as a function of real k when $\Delta V = 5.0$, and $\delta = 0.1$. These results are reproduced from

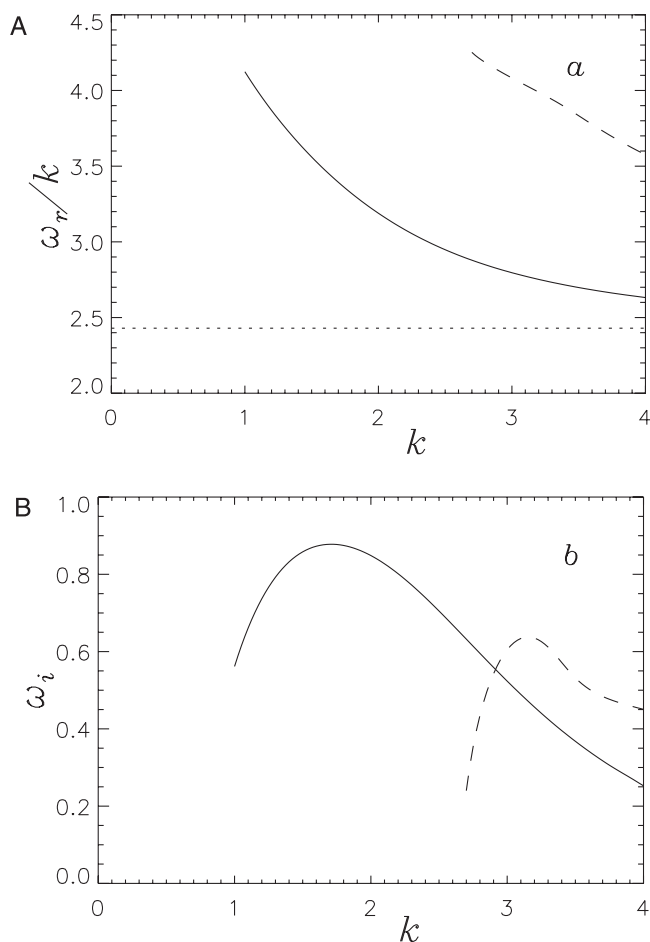


Figure 7. The dispersion relations of the fundamental (solid line) and second harmonic (dashed line) waveguide modes. The dotted line is the fast speed in the magnetosphere, to which the ω_r/k tends for large k ($\Delta V = 5.0$, $\delta = 0.1$).

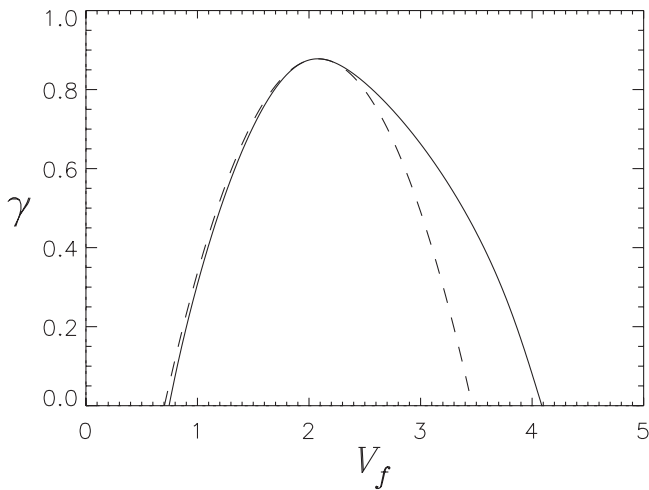


Figure 8. Same format as Figure 5, but for the fundamental waveguide mode disturbances ($\Delta V = 5.0$, $\delta = 0.1$).

some of the information displayed in the work of *Mills et al.* [2000, Figure 7]. From these numerical solutions we find the following values for the fundamental and second harmonic, respectively: $k_m = 1.70, 3.15$; $\omega_{rm} = 5.77, 12.64$; $\omega_{im} = 0.8778, 0.6378$; $V_g = 2.084, 2.553$; $\partial^2 \omega_r(k_m)/\partial k^2 = -0.4707, -1.0284$; $\partial^2 \omega_i(k_m)/\partial k^2 = -0.8085, -2.6449$; $a = 1.8432, 0.6569$; $b = 1.0766, 0.2554$.

[33] The double root analysis results for these modes are given by *Mills et al.* [2000, Figure 13] which confirms these modes are convectively unstable in the magnetospheric rest frame ($V_f = 0$). In Figure 8 we reproduce their solution for the fundamental mode (solid line) and compare with the wave packet estimate (dashed line) of (15). Good agreement is found for $V_f < 2$, but for $V_f > 2$ some differences arise due to the fact that the curves in Figure 7 are not approximated very accurately by quadratic functions far away from k_m . Nevertheless, our approximate result gives a reasonable estimate of the range of V_f for which absolute and convective instabilities occur.

[34] Now that we have a reasonable idea of the types of wave packets that can be produced it is interesting to study the FLRs (Alfvén waves) that they may excite, especially as the latter are readily observable. To do this calculation properly would require a nonuniform magnetosphere and recalculation of the dispersion relations for the new normal modes that correspond to waveguide modes coupled to an FLR. Such calculations have been done elsewhere [*Fujita et al.*, 1996; *Mills and Wright*, 1999] and the properties inferred from these dispersion relations do not differ significantly from those given here. Since we are only attempting to indicate the basic properties of FLRs in this section, we use the fields (10) and (11) to excite the FLRs. A more complete and consistent calculation is left for a future study. It would also be desirable to include the three-dimensional nature of the flank in future investigations.

[35] The fast waveguide mode wave packets will couple to FLRs (Alfvén waves) as they propagate around the flanks and into the magnetotail. *Wright* [1992a] shows how this low k coupling process can be approximated by representing the Alfvén wave fields as satisfying a simple harmonic oscillator equation that is driven by a time-dependent

function representing the fast mode, such as ξ_x (the plasma displacement along x) or v_x (the plasma velocity along x). We can produce just this driving function by taking (10) and (11) which describe the fast mode disturbance and evaluating them on a given magnetospheric field line ($y = \text{constant}$) as a function of time.

[36] FLRs occur over a range of magnetic local times from 4 to 20 hours. During strong solar wind conditions (speed $> 500 \text{ km s}^{-1}$) we expect the subsolar magnetopause to be leaky for magnetospheric waveguide modes. As the flow speed increases away from noon the magnetopause provides a perfect reflector, and when it exceeds 400 to 500 km s^{-1} on the flanks the waveguide modes become Kelvin–Helmholtz unstable. Thus it is likely that there will be an equatorial extent of magnetopause of at least $5 R_E$ from noon before the waveguide modes become unstable. A further $10 R_E$ would take us to roughly 8 or 16 MLT, and another $10 R_E$ would correspond to predawn/postdusk MLT. To investigate the waveguide mode fields at these local times we consider the wave packet evolution after propagating $10 R_E$ and $20 R_E$ down the waveguide. (In normalized units this corresponds to $y = 1.0$ and 2.0 , respectively.)

[37] Figure 9 shows the waveguide mode fields for a fundamental mode wave packet launched from $y = 0$ at $t = 0$

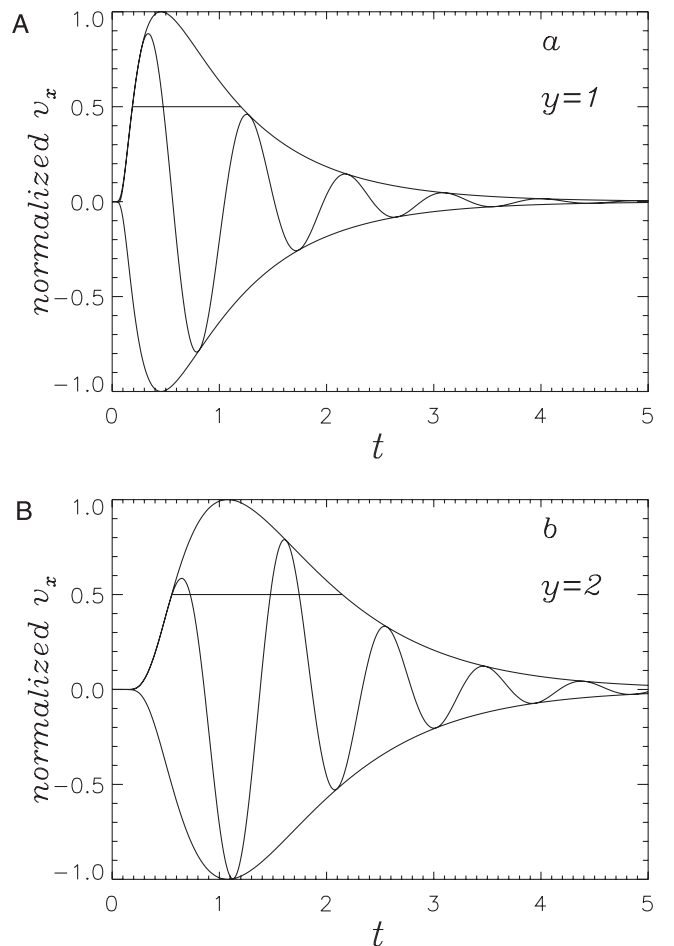


Figure 9. The time variation of wave packet fields as the fundamental wave packet passes over the field line (a) $y = 1.0$ and (b) $y = 2.0$. The envelope is based upon (10) and the full width at half maximum is indicated.

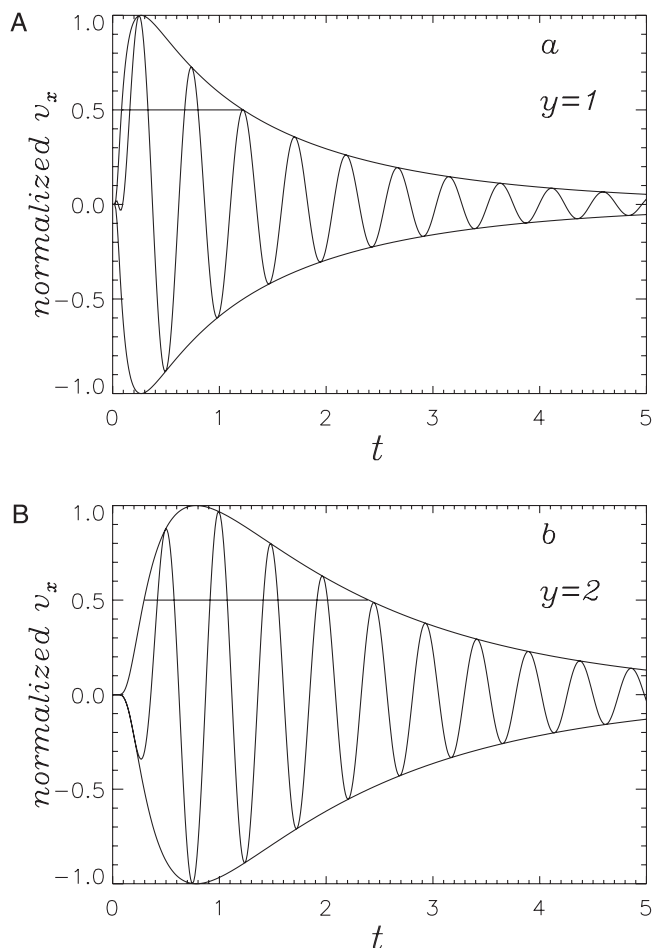


Figure 10. The same as Figure 9, but for the second harmonic wave packet.

when the wave packet passes over (a) $y = 1.0$, and (b) $y = 2.0$ according to the result in (10) and (11). Both the envelope and the phase oscillations are shown. The horizontal line marks the full width at half maximum of the envelope ($\tau(y)$). A rough estimate of the number of cycles (n) that the Alfvén waves are driven for is simply $\omega_{rm}\tau(y)/2\pi$, and for Figure 9a this gives $n \approx 0.9$.

[38] Wright [1992b] and Mann *et al.* [1995] show how the longer an Alfvén resonance is excited for (i.e., the greater n is) the narrower the frequency spectrum of the driver and the narrower the width of the Alfvén resonance. Allan and Wright [1997] included ionospheric dissipation effects in addition, and calculated the width of Alfvén resonances as a function of time and the asymptotic limit due to dissipation. Allan and Wright [1997, Table 1 and Figures 3 and 4] give typical parameters for FLRs. Using these results we predict the FLR driven by the fundamental waveguide mode wave packet for $n \sim 1$ cycle to have a radial scale in the equatorial plane of 4 or 5 R_E . This is very broad, and FLRs typically have equatorial widths of 0.5 R_E .

[39] Figure 9b shows the fundamental mode wave packet further down the flank ($y = 2$) compared to that in Figure 9a. The wave packet has broadened but the half width calculation suggests that $n \sim 1.5$. Allan and Wright [1997] show that if the height integrated Pedersen conductivity (Σ_p) is

0.8 S the fundamental driven FLR has an asymptotic width of 1.5 R_E , and will need to be driven for 4 cycles to phase mix down to this length.

[40] Figure 10 displays the same results as in Figure 9, but is for the second harmonic wave packet. The half-width calculation gives $n \sim 2.3$ at $y = 1.0$ and $n \sim 4.2$ at $y = 2.0$. Allan and Wright [1997] show that for $\Sigma_p \approx 0.85$ the second harmonic driven FLR needs to be driven for 3 to 4 cycles to narrow to its asymptotic width of $\sim 1 R_E$. Thus it is more likely that the second harmonic wave packets will drive a fully developed FLR in the predawn/postdusk sectors.

[41] The fact that the fundamental waveguide mode wave packet in Figure 9a provides a much broader band driver than more numerous oscillations in Figure 10b is demonstrated by taking the temporal Fourier transform of these signals, the results are shown in Figure 11. The ratio of the width of the peak ($\Delta\omega$) to the central frequency scales as $1/n$. For the broad band driver in Figure 9a the Fourier transform in Figure 11a has $\Delta\omega/\omega \sim 1$. Whereas the more monochromatic signal in Figure 10b has the Fourier transform in Figure 11b with $\Delta\omega/\omega \sim 1/4.5$.

[42] A close inspection of Figures 11a and 11b shows the peaks to be located at $\omega = 6.7$ and 13.0, respectively. These values are slightly different to ω_{rm} for the fundamental and second harmonic modes (5.77 and 12.64, respectively). The

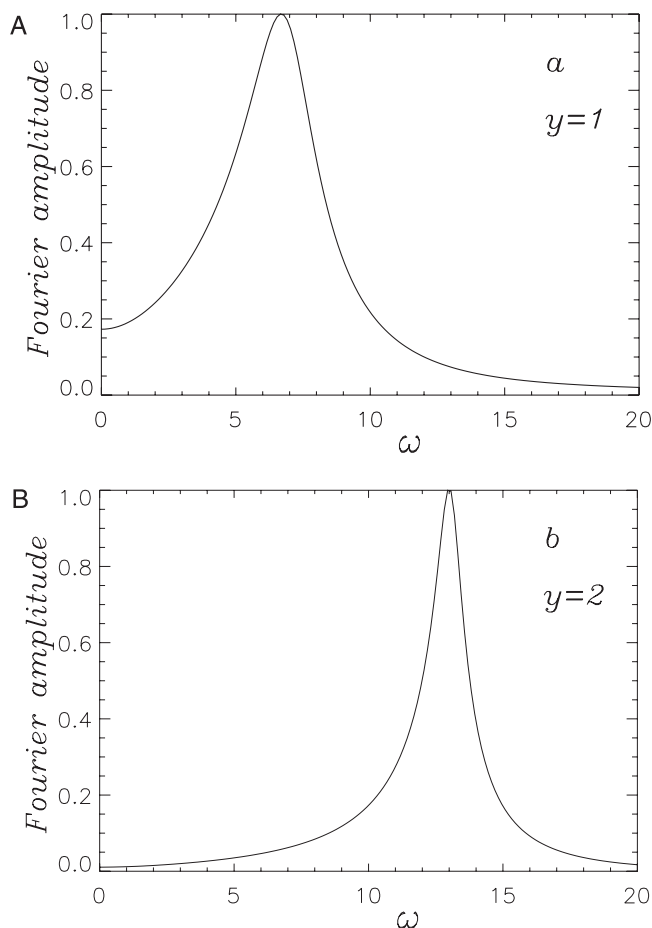


Figure 11. The frequency spectrum of (a) the signal in Figure 9a and (b) the signal in Figure 10b.

difference may be accounted for by a more careful calculation of the instantaneous frequency using (11);

$$\omega = -\frac{\partial\phi}{\partial t} = \omega_{rm} + \frac{bV_g^2}{4} - \frac{by^2}{4t^2} \quad (23)$$

For the moment we shall neglect the final term in (23) and find revised frequency estimates of 6.9 and 13.05, respectively, based upon the first two terms on the right hand side of (23). These values are in much better agreement with the values inferred from Figure 11. The small remaining discrepancy can be accounted for by the final term, which requires us to specify a time. Since the FFT in Figure 11 is not calculated at a particular time, but over a time interval, an exact correction is not simple. However, we could argue that $t = 1.0$ is representative of the center of the signal in Figure 9a, and similarly $t = 2.0$ for Figure 10b. Thus the final term in (23) suggests the preliminary frequency estimates of 6.9 and 13.05 should be reduced by an amount of roughly 0.27 and 0.06 which would then give excellent agreement with the values inferred from Figure 11.

[43] A free parameter in our calculation is δ , the half width of the velocity shear layer. In the simulation and discussion so far we have taken $\delta = 0.1$ (i.e., $1 R_E$), partly for numerical convenience. On some occasions the layer may be slightly thinner, say, $\delta = 0.05$, and we have recomputed the above results for this value. Here we only summarize results. The values quoted in parentheses are the $\delta = 0.1$ values found earlier, and are included here for comparison only.

[44] For the fundamental we find $k_m = 2.225$ (1.70); $\omega_{rm} = 7.075$ (5.77); $\omega_{im} = 1.225$ (0.8778); $V_g = 1.980$ (2.084); $a = 2.946$ (1.843); $b = 1.433$ (1.0766). At $y = 1.0$ a wave packet will supply 1.0 (1.0) driving cycles, and at $y = 2.0$ about 1.6 (1.5) cycles. For the second harmonic the results are $k_m = 3.70$ (3.15); $\omega_{rm} = 14.04$ (12.64); $\omega_{im} = 1.004$ (0.6378); $V_g = 2.198$ (2.553); $a = 1.279$ (0.6569); $b = 1.533$ (0.2554). At $y = 1.0$ a wave packet will supply 3.0 (2.3) driving cycles, and at $y = 2.0$ about 5.2 (4.2) cycles. Thus it appears that the number of driving cycles supplied by a waveguide mode wave packet is fairly insensitive to the width of the shear layer.

[45] We conclude this section with some comments regarding the amplitude of the waveguide modes that may excite FLRs. As already established the e-folding length of these waveguide modes is large ($\sim 20 R_E$) suggesting their amplitude remains small and enables us to treat them using linear theory. Waveguide and cavity modes are surprisingly elusive in data, and it is generally believed that they are of such small amplitude as to be undetectable by today's observing missions and analysis methods. Indeed, it was not direct observation of these modes that has led to their popularity over the last two decades, rather it is the existence and observed properties of FLRs that led theorists to postulate their existence as necessary [Kivelson and Southwood, 1985].

[46] Why is it that FLRs have a significantly larger amplitude than the fast modes that excite them? The answer lies in the different behavior of the two modes: The fast mode propagates and disperses across field lines on the flanks and travels into the magnetotail. FLRs are Alfvén

waves whose energy is focused on a restricted range of L-shells and, importantly, remains on the same field lines. The Alfvén wave energy on closed flank field lines will not propagate into the tail. Moreover, subsequent excitation by a new wave packet will add to the amplitude and energy of the FLR. For example, in the limit of a steady harmonic excitation commencing at $t = 0$, the FLR amplitude grows $\propto t$ even for a fixed small amplitude driver [Wright, 1992a, 1992b]. (The FLR amplitude will not grow indefinitely in practice because of ionospheric dissipation.) Thus it is not necessarily the case that a large amplitude FLR need be excited by a large amplitude (and readily observable) fast mode—and observations indicate that this is generally the case.

6. Discussion and Conclusions

[47] In the previous section we have identified the properties of convectively unstable waveguide mode wave packets. This has been the main aim of the present study. To illustrate how the ideas we have developed may be used to gain a better understanding of how the magnetosheath and magnetosphere are coupled we also considered the expected properties of FLRs that unstable waveguide mode wave packets would excite. The next two subsections summarize and interpret observations of FLRs. Although FLR excitation is not the main focus of this paper, this is an opportunity to show how two areas that are studied separately may be related—something that is often very fruitful.

6.1. Observations

[48] Observations of waveguide modes and wave packets are elusive, although Mann *et al.* [1998] report a rare multisatellite observation showing antisunward propagation. One spacecraft was located near noon and the other at 9 MLT. It is unlikely that the waveguide modes were KH unstable at noon, and at 9 MLT they may have just turned unstable, although a perfectly reflecting magnetopause is more likely. This is supported by the fact that the satellite fields at 9 MLT show no amplification from those at noon, and are in fact slightly reduced in amplitude. This property is consistent with waveguide dispersion [Wright, 1994]. The EISCAT cross (also near noon) saw the waveguide mode fields also, but no FLR, possibly because the driver was not coherent enough.

[49] The unstable convecting wave packets this paper focuses on have a special feature in the FLRs they excite: As shown by Mills and Wright [1999] and Mann and Wright [1999] the Kelvin–Helmholtz mechanism will be able to excite two or more FLRs simultaneously that have a common azimuthal phase speed. Mathie and Mann [2000] used the IMAGE magnetometer array to find multiple FLR events and classified them as “common phase speed” (CPS) or “independent phase speed” (IPS). Their Figure 11 shows a remarkable pattern in the distribution of these events with MLT. The CPS distribution had a gap around noon (11 to 13 MLT) and peaked on both flanks at 9 and 15 MLT. This is in agreement with the KH mechanism we propose: As noted by Mann and Wright [1999] the low magnetopause velocity shear near noon means the waveguide modes are stable here, whereas on the flanks they are more likely to be unstable. (The IPS events, which could be

driven by impulsive or random buffeting of the magnetosphere, show a more uniform distribution from 5 to 15 MLT.)

6.2. Interpretation

[50] The CPS events occurring around 8 and 16 MLT would probably experience wave packets like those in Figures 9a and 10a. Even under favorable conditions these local times would struggle to see wave packets that provide more than a couple of driving cycles. The CPS events closer to noon (at 10 or 14 MLT) are very close to where the waveguide modes become unstable, and any wave packets would have had little time to broaden at these locations. This indicates that the continually driven wave train is a more likely driver of these CPS events, and raises the question of what could produce a suitable steady oscillatory source at the beginning of the unstable section of waveguide? It could well be that the waveguide modes which propagate and disperse down the sunward section of reflecting waveguide provide an ideal seed for an unstable waveguide mode wave train as they reach the unstable section. Of course, a steady spatially growing wave train can also be thought of a superposition of propagating wave packets [see Mills *et al.*, 2000, Figure 12]. Although one wave packet may not drive a narrow fully formed resonance, it is possible that several consecutive wave packets could, so long as their separation did not exceed the ionospheric dissipation timescale.

[51] The present wave packet analysis assumes that the wave packet begins with negligible width. One way of producing a wave packet that gives more driving cycles is to start off with a wave packet of finite extent Δy at the beginning of the unstable waveguide section. If the initial width is to produce an extra N cycles of the driver, we may relate N , V_g and ω_{rm} by $\Delta y \approx 2N\pi V_g/\omega_{rm}$. A modest increase with $N = 2$ would require $\Delta y = 4.5$ and 2.5 (45 and $25 R_E$ in dimensional units) for the fundamental and second harmonic modes. This large extent means the whole of the flank would be disturbed initially, and such a situation is more reasonably described as a wave train, rather than a very broad wave packet.

6.3. Summary

[52] We have presented an analytical approximation to the convectively unstable wave packets that are thought to exist on the convectively unstable magnetospheric flanks. Our approximation is shown to be in good agreement with numerical results. One interpretation of the convective instability is in terms of a propagating, growing and broadening wave packet, and we show how the standard results may be recovered. Another interpretation is that of a steady source that radiates a wave train whose amplitude grows exponentially with distance from the source. We try to decide which picture is the most approximate for the magnetospheric flanks, since this will help identify the dominant processes that couple the magnetosheath and magnetosphere.

[53] As wave packets propagate antisunward they broaden. Thus the further antisunward a magnetospheric field line is the more driving cycles it will see. This suggests that wave packets will drive narrower (in L-shell) FLRs on these field lines compared to their sunward counterparts

[Mann *et al.*, 1995]. Our estimates show that a single wave packet of the fundamental mode will not drive fully formed narrow FLRs on the dayside. The trend is for higher harmonic waveguide mode wave packets to provide more driving cycles, but the second harmonic only gives 2–3 driving cycles. So we expect fully developed FLRs here to be driven by a wave train or multiple wave packets.

[54] FLRs further round on the flanks may be driven by higher harmonic waveguide mode wave packets. For the second harmonic, favorable conditions may allow it to drive a fully developed FLR, but it is likely that fundamental and second harmonic waveguide modes will need to drive as a wave train or as successive wave packets even here.

[55] It is likely that wave trains of the convectively unstable waveguide modes will be important in driving FLRs. Such wave trains may well be excited by the propagation of trapped waveguide modes from the sunward reflecting section of waveguide into the KH unstable section.

[56] **Acknowledgments.** This work was completed in part while ANW was a UK PPARC Advanced Fellow, KJM was a PPARC student, and both AWL and MSR were PPARC postdocs.

References

- Allan, W., and A. N. Wright, Large- m waves generated by small- m field line resonances via the nonlinear Kelvin–Helmholtz instability, *J. Geophys. Res.*, *102*, 19,927, 1997.
- Bers, A., Space–time evolution of plasma instabilities: Absolute and convective, in *Handbook of Plasma Physics I, Vol. 1, Basic Plasma Physics I*, edited by M. N. Rosenbluth and R. Z. Sagdeev, p. 1, North-Holland, New York, 1983.
- Briggs, R. J., *Electron–Stream Interaction With Plasmas*, Res. Monogr. No. 29, MIT Press, Cambridge, Mass., 1964.
- Chen, L., and A. Hasegawa, A theory of long-period magnetic pulsations, 1, Steady state excitation of field line resonance, *J. Geophys. Res.*, *79*, 1024, 1974.
- Engebretson, M., K.-H. Glassmeier, M. Stellmacher, W. J. Hughes, and H. Luhr, The dependence of high-latitude Pc5 wave power on solar wind velocity and on the phase of high speed solar wind streams, *J. Geophys. Res.*, *103*, 26,271, 1998.
- Fenrich, F. R., J. C. Samson, G. Sofko, and R. A. Greenwald, ULF high- and low- m field line resonances observed with the Super Dual Auroral Radar Network, *J. Geophys. Res.*, *100*, 21,535, 1995.
- Fujita, S., K.-H. Glassmeier, and K. Kamide, MHD waves generated by the Kelvin–Helmholtz instability in a nonuniform magnetosphere, *J. Geophys. Res.*, *101*, 27,317, 1996.
- Keller, K. A., and R. L. Lysak, MHD simulation of magnetospheric waveguide modes, *J. Geophys. Res.*, *106*, 8447, 2001.
- Kivelson, M. G., and D. J. Southwood, Resonant ULF waves: A new interpretation, *Geophys. Res. Lett.*, *12*, 49, 1985.
- McKenzie, J. F., Hydromagnetic wave interaction with the magnetopause and the bow shock, *Planet. Space Sci.*, *18*, 1, 1970.
- Mann, I. R., and A. N. Wright, Diagnosing the excitation mechanisms of Pc5 magnetospheric flank waveguide mode and FLRs, *Geophys. Res. Lett.*, *26*, 2609, 1999.
- Mann, I. R., A. N. Wright, and P. S. Cally, Coupling of magnetospheric cavity modes to field line resonances: A study of resonance widths, *J. Geophys. Res.*, *100*, 19,441, 1995.
- Mann, I. R., G. Chisham, and S. D. Bale, Multisatellite and ground-based observations of a tailward propagating Pc5 magnetospheric waveguide mode, *J. Geophys. Res.*, *103*, 4657, 1998.
- Mann, I. R., A. N. Wright, K. J. Mills, and V. M. Nakariakov, Excitation of magnetospheric waveguide modes by the magnetosheath flow, *J. Geophys. Res.*, *104*, 333, 1999.
- Manuel, J. R., and J. C. Samson, The spatial development of the low latitude boundary layer, *J. Geophys. Res.*, *98*, 17,367, 1993.
- Mathie, R. A., and I. R. Mann, Observations of Pc5 field line resonance azimuthal phase speeds: A diagnostic of their excitation mechanism, *J. Geophys. Res.*, *105*, 10,713, 2000.
- Mills, K. J., and A. N. Wright, Azimuthal phase speeds of field line resonances driven by Kelvin–Helmholtz unstable waveguide modes, *J. Geophys. Res.*, *104*, 22,667, 1999.

- Mills, K. J., A. N. Wright, and I. R. Mann, Kelvin–Helmholtz driven modes of the magnetosphere, *Phys. Plasmas*, 6, 4070, 1999.
- Mills, K. J., A. W. Longbottom, A. N. Wright, and M. S. Ruderman, The Kelvin–Helmholtz instability of the magnetospheric flanks: An absolute and convective instability approach, *J. Geophys. Res.*, 105, 27,685, 2000.
- Miura, A., Anomalous transport by magnetohydrodynamic Kelvin–Helmholtz instabilities in the solar wind–magnetosphere interaction, *J. Geophys. Res.*, 89, 801, 1984.
- Miura, A., Simulation of Kelvin–Helmholtz instability at the magnetosphere boundary, *J. Geophys. Res.*, 92, 3195, 1987.
- Miura, A., Kelvin–Helmholtz instability at the magnetospheric boundary: Dependence on the magnetosheath sonic Mach number, *J. Geophys. Res.*, 97, 10,655, 1992.
- Miura, A., Kelvin–Helmholtz instability at the magnetopause: Computer simulations, in *Physics of the Magnetopause*, *Geophys. Monogr. Ser.*, vol. 90, edited by P. Song et al., p. 285, AGU, Washington, D. C., 1995.
- Miura, A., A quantitative test of the self-organization hypothesis of the magnetopause Kelvin–Helmholtz instability as an inverse problem, *Geophys. Res. Lett.*, 26, 409, 1999.
- Miura, A., and P. L. Pritchett, Nonlocal stability analysis of the MHD Kelvin–Helmholtz instability in a compressible plasma, *J. Geophys. Res.*, 87, 7431, 1982.
- Samson, J. C., J. A. Jacobs, and G. Rostoker, Latitude-dependent characteristics of long-period geomagnetic micropulsations, *J. Geophys. Res.*, 76, 3675, 1971.
- Samson, J. C., B. G. Harrold, J. M. Ruohoniemi, and A. D. M. Walker, Field line resonances associated with MHD waveguides in the magnetosphere, *Geophys. Res. Lett.*, 19, 441, 1992.
- Southwood, D. J., The hydromagnetic stability of the magnetospheric boundary, *Planet. Space Sci.*, 16, 587, 1968.
- Southwood, D. J., Some features of field line resonances in the magnetosphere, *Planet. Space Sci.*, 22, 483, 1974.
- Walker, A. D. M., The Kelvin–Helmholtz instability in the low-latitude boundary layer, *Planet. Space Sci.*, 29, 293, 1981.
- Walker, A. D. M., Excitation of magnetohydrodynamic cavities in the magnetosphere, *J. Atmos. Sol.-Terr. Phys.*, 60, 1279, 1998.
- Walker, A. D. M., J. M. Ruohoniemi, K. B. Baker, R. A. Greenwald, and J. C. Samson, Spatial and temporal behaviour of ULF pulsations observed by the Goose Bay HF radar, *J. Geophys. Res.*, 97, 12,187, 1992.
- Wright, A. N., Coupling of fast and Alfvén modes in realistic magnetospheric geometries, *J. Geophys. Res.*, 97, 6429, 1992a.
- Wright, A. N., Asymptotic and time-dependent solutions of magnetic pulsations in realistic magnetic field geometries, *J. Geophys. Res.*, 97, 6439, 1992b.
- Wright, A. N., Dispersion and wave coupling in inhomogeneous MHD waveguides, *J. Geophys. Res.*, 99, 159, 1994.
- Wright, A. N., K. J. Mills, M. S. Ruderman, and L. Brevdo, The absolute and convective instability of the magnetospheric flanks, *J. Geophys. Res.*, 105, 385, 2000.
- Wu, C. C., Kelvin–Helmholtz instability at the magnetopause boundary, *J. Geophys. Res.*, 91, 3042, 1986.
- Ziesolleck, C. W. S., and D. R. McDiarmid, Auroral latitude Pc5 field line resonances: Quantized frequencies, spatial characteristics, and diurnal variation, *J. Geophys. Res.*, 99, 5817, 1994.

A. N. Wright, Department of Mathematical and Computational Sciences, Mathematical Institute, Room M212, University of St. Andrews, North Haugh, St. Andrews, Fife KY16 9SS, UK. (andy@mcs.st-and.ac.uk)

K. J. Mills, Thompson Marconi Sonar Ltd., Dolphin House, Ashurst Drive, Cheadle Heath, Stockport, Cheshire, SK3 0XB, UK.

A. W. Longbottom, Fluid Gravity Engineering Ltd., 83 Market Street, St. Andrews, Fife, KY16 9NX, UK.

M. S. Ruderman, Department of Applied Mathematics, University of Sheffield, Hicks Building, Western Bank, Sheffield S3 7RH, UK.